Glass Europe Vol. 2 (2024) 137-149
https://doi.org/10.52825/glass-europe.v2i.976

Submitted: 18 Dec. 2023 | Accepted: 30 Jul. 2024 | Published: 14 Nov. 2024

A New Model for Describing the Glass to Metal Interaction in Forming

Christian Roos[1], Jan-Hendrik Veltmaat[1], and Philipp Jacobs[1,*]

[1] RWTH Aachen University, Germany

*Correspondence: Philipp Jacobs, jacobs@ghi.rwth-aachen.de

Abstract. The interaction between molten glass and metallic molds plays a crucial role in industrial glass-forming. Glass-metal sticking is usually described in terms of material- and process-dependent "sticking temperatures"; however, these parameters tell little about the underlying physical processes such as adhesion, wetting and spreading. We show that the molecular-kinetic spreading model, originally developed for liquids at room temperature, is also valid for a droplet of molten glass on different substrate materials: Measured contact angles and spreading velocities yield plausible values for the molecular jump rate $k_s \approx 10^{12}$ Hz and jump distance $\lambda \approx 3$–6 Å. In addition, we argue that the real-world glass–metal contact is actually the contact between a liquid oxide (the glass melt) and a solid oxide (the metal's oxide layer). The spatial dominance of oxygen ions might explain why sticking temperatures appear to be only weakly dependent on the contact material's chemical composition. Both findings lead us to the conclusion that the current theory of glass-metal interaction should be revisited.

Keywords: Glass-Metal Contact, Sticking Temperatures, Wetting, Spreading, Interface Viscosity, Molecular Kinetic Model, Metal Oxides

1. Introduction and theoretical considerations

Industrial glass-forming usually relies on molds that can withstand direct contact with molten glass. Although cast iron has established itself as a mold material, protective coatings or lubricants are still required to mitigate thermal stress, wear and glass sticking. Especially sticking is to be avoided for a reliable production of glass containers (see Figure 1). However, liquid lubricants tend to cause contamination and corrosion. As these suspensions often contain graphite and sulfur, they also pose a health risk to workers who manually "swab" the molds [1]. A better understanding of the glass–metal contact is thus essential for a more reliable and safer glass-forming process.

Research on glass sticking dates back at least as far as the mid-1960s and has since led to the definition of several material- and process-dependent "sticking temperatures" [2], [3], [4], [5]. Rieser et al. [6] propose a lower sticking temperature (LST) and an upper sticking temperature (UST), based on the results of industry-oriented experiments. The LST marks the onset of glass sticking, whereas the UST is characterized by the fact that a damage-free separation of the (cooled) glass and the metal is no longer possible (here, both the lower and the upper sticking temperature refer to the temperature of the metal before it comes into contact with molten glass). By analyzing the temperature–viscosity curve of a silicate glass melt, Rieser et al. link its LST with a material-independent "contact viscosity" of $\eta_c \approx 10^{8.8}$ Pa·s: Molten glass sticks at viscosities $\eta \leq \eta_c$, regardless of the metal it is in contact with. Consequently, the lower sticking temperature depends mainly on the thermal properties of the contact material. The

corresponding heat penetration coefficient or thermal effusivity $b = \sqrt{\lambda \cdot c_\mathrm{p} \cdot \rho}$ is given by the metal's specific heat capacity c_p, thermal conductivity λ and density ρ [7], [8]. Molten glass will stick more readily to a material with a lower thermal effusivity b, because the temperature T (or its equivalent viscosity η) of the glass melt at the interface remains higher (lower, i.e. below η_c) for longer. This only holds true as long as the contact material's temperature is lower than the temperature of the glass.

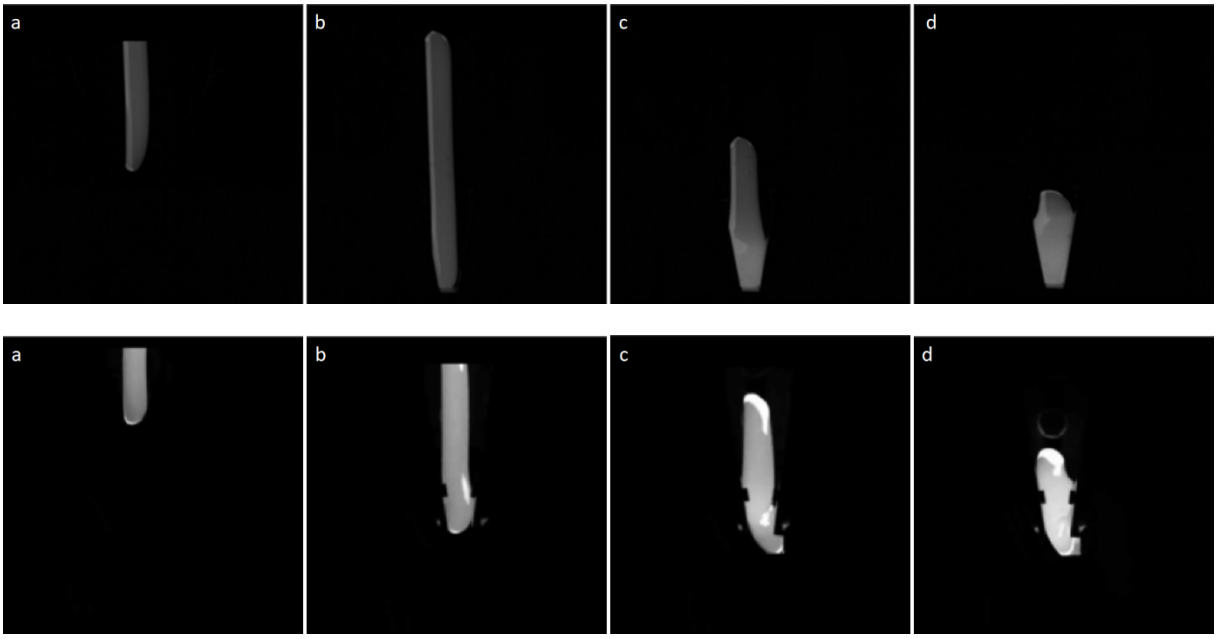

***Figure 1**. A sticking-free glass–metal contact is crucial for the successful loading of a glass gob into a container mold. The ideal case is shown in the upper picture sequence: (a) The glass gob arrives and (b) comes into contact with the mold. (c) After sliding along the mold walls, (d) the molten glass fills the mold symmetrically. In contrast, the impact of sticking is shown in the lower picture sequence: (a) The glass gob arrives, (b) comes into contact with one of the mold walls and (c) sticks to it. (d) As a result, the molten glass is not evenly distributed in the mold. Further information can be found in [8].*

Although sticking temperatures are useful parameters for characterizing the industrial glass-forming process, they do not take into account dynamic friction and other relevant aspects. The influence of dynamic friction on glass sticking was investigated by us in a previous paper [8]. Furthermore, Heilmann and Rigney developed an energy-based approach to frictional contact [9], [10], [11]. In their theory, the coefficient of friction $\mu \propto \frac{A_\mathrm{c} N \tau_\mathrm{max}}{P}$ depends on the contact area A_c, number of contacts N, maximum shear strength τ_max and applied load P.

At its core, the glass–metal contact is about the interaction between a (viscoelastic) liquid and a solid. The associated phenomena such as adhesion, wetting and spreading are well researched, at least in the case of liquids at room temperature [12], [13], [14], [15], [16]: Figure 2 shows a liquid (L) droplet on a solid (S) surface that is surrounded by a gaseous (V) phase.

The tension at the solid–liquid interface σ_SL depends not only on the surface tensions σ_SV and σ_LV, but also on the "work of adhesion" W_SL:

$$\sigma_{SL} = \sigma_\mathrm{SV} + \sigma_\mathrm{LV} - W_\mathrm{SL} \quad \Leftrightarrow \quad W_\mathrm{SL} = \sigma_\mathrm{SV} + \sigma_\mathrm{LV} - \sigma_\mathrm{SL} \tag{1}$$

The "work of adhesion" W_SL (as well as any interface tension σ) can be interpreted as a force per unit length (in $\mathrm{N \cdot m^{-1}}$) or, equivalently, as an energy per unit area (in $\mathrm{J \cdot m^{-2}}$). At the contact line where all three phases meet, the surfaces of the droplet and the substrate form the contact angle θ. In thermodynamic equilibrium, the static contact angle θ_s is the result of

balanced interface tensions (this balance of forces is only considered in the horizontal direction. The equilibrium in the vertical direction involves the Laplace pressure [16], which is not considered here):

$$\sigma_{\mathrm{SV}} - \sigma_{\mathrm{SL}} = \sigma_{\mathrm{LV}} \cdot \cos\theta_{\mathrm{s}} \tag{2}$$

Combining equations 1 and 2 yields the Young–Dupré equation:

$$W_{\mathrm{SL}} = \sigma_{\mathrm{LV}} \cdot (1 + \cos\theta_{\mathrm{s}}) \tag{3}$$

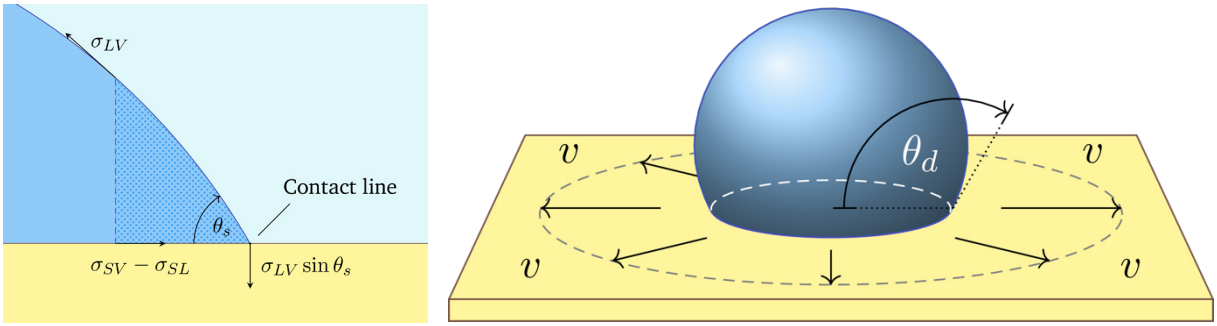

***Figure 2**. A liquid droplet (blue) on a solid surface (yellow). In thermodynamic equilibrium (left), the interface tensions σ_{SV}, σ_{LV} and σ_{SL} are balanced and the contact angle θ_s is static [16]. In contrast, the (dynamic) contact angle θ_d changes during spreading (right) and the contact line (white dashes) moves in radial direction at the spreading velocity v.*

The contact angle θ is the key value for quantifying wetting or adhesion: According to equation 3, a smaller static contact angle θ_s relates to stronger adhesion (W_{SL}) and pronounced wetting [12]. This relation applies regardless of what interaction causes the attraction between the condensed phases. For example, if neither the liquid nor the solid contains permanent dipoles—which can be assumed in our case—the only remaining van der Waals interaction is the London dispersion force:

$$W_{\mathrm{SL}} = W(r)_{\mathrm{London}} = -\frac{3}{2}\frac{\alpha_{01}\alpha_{02}}{(4\pi\varepsilon_0)^2 r^6}\frac{I_1 I_2}{I_1 + I_2} \tag{4}$$

where the respective ionization potentials I and polarizabilities α refer to two atoms or molecules that are separated by a distance r while ε_0 is the vacuum permittivity. The London dispersion force results from an asymmetric electron density within a (normally symmetric) atom or molecule. This fluctuation can occur spontaneously or be induced by another temporary dipole [17].

The above discussion of wetting was limited to thermodynamic equilibrium. In practice, a droplet usually "spreads" for some time before it reaches a stable shape (see Figure 2). Blake and Haynes' molecular-kinetic model describes this process on a microscopic scale [18], [19]. More precisely, their model considers spreading to be the result of (forced) molecular movement in the solid–liquid–vapor region or contact "line". The radial velocity v of the contact line is the spreading velocity

$$v = \lambda \cdot (k_+ - k_-), \tag{5}$$

with λ being the jump distance of the liquid's molecules; k_+ and k_- denote the jump rates in the forward and reverse directions, respectively. Borrowing from Eyring's reaction rate theory, Blake and Haynes state

$$k_\pm = \frac{k_{\mathrm{B}} \cdot T}{h} \exp\left(-\frac{\Delta G_{\mathrm{s}} + \Delta G_\eta \pm W}{k_{\mathrm{B}} \cdot T}\right) \tag{6}$$

where k_B and h denote the Boltzmann and Planck constant, respectively. Besides the temperature T, the jump rate $k_\pm$ is controlled by an activation energy whose first two contributions are ΔG_s and ΔG_η. The third term $W = \frac{F \cdot \lambda}{2}$ is the work of the force F that results from unbalanced interface tensions (see equation 2):

$$F = \lambda \cdot (\sigma_{SV} - \sigma_{SL} - \sigma_{LV} \cdot \cos\theta_d) = \lambda \cdot \sigma_{LV} \cdot (\cos\theta_s - \cos\theta_d) \quad (7)$$

The force F drives spreading as long as the time-dependent dynamic contact angle θ_d has not reached its equilibrium (static) value θ_s. Taking into account the definition of the dynamic viscosity $\eta = \frac{h}{\lambda^3} \cdot \exp\left(\frac{\Delta G_\eta}{k_B \cdot T}\right)$ [19], equations 5–7 yield

$$v = 2\frac{h}{\lambda^2 \eta} k_s \sinh\left(\frac{\lambda^2 \sigma_{lv}(\cos\theta_s - \cos\theta_d)}{2 k_B T}\right) \quad (8)$$

with the direction-independent jump rate

$$k_s = \frac{k_B T}{h} \exp\left(-\frac{\Delta G_S}{k_B T}\right) \quad (9)$$

In fluid dynamics, forces acting on liquids are often expressed in terms of dimensionless quantities. One such quantity is the capillary number $\mathrm{Ca} = \frac{\eta \cdot v}{\sigma_{LV}}$, which represents the ratio of viscous drag forces to surface tension [12]. Equation 8 can be rewritten accordingly:

$$\mathrm{Ca} = 2\frac{h}{\lambda^2 \sigma_{lv}} k_s \sinh\frac{\lambda^2 \sigma_{lv}(\cos\theta_s - \cos\theta_d)}{2 k_B T} \quad (10)$$

Due to the semi-empirical nature of the molecular-kinetic model, the jump rate k_s and jump distance λ can only be determined using experimental data: By fitting equation 10 to measured spreading velocities v and contact angles (θ_s as well as θ_d), the microscopic quantities k_s and λ become accessible.

2. Experimental

In a series of isothermal experiments, the spreading of a glass droplet on different substrate materials was investigated. All experiments were carried out with a conventional soda–lime–silica glass (SLS glass); its main constituents are 71.6 wt% SiO_2, 13.7 wt% Na_2O, 11.1 wt% CaO, 1.9 wt% Al_2O_3 and 0.8 wt% MgO. The properties of the glass can be determined using statistical models: Fluegel's models [20], [21], [22] provides the temperature–viscosity curve η(T) and temperature–density curve ρ(T), while Kucuk's model [23] yields the surface tension σ_{LV}(1400 °C) = 316.98 mN·m^{-1}. In addition, Salmang [24] states the temperature dependence of the surface tension as $\frac{d\sigma_{LV}}{dT} \approx -0.04$ mN·m^{-1}·K^{-1}. Table 1 summarizes all relevant glass properties.

***Table 1**. Viscosity η, density ρ and surface tension σ_{GV} of the glass at temperature T.*

T (°C)	η (dPa·s)	ρ (g·cm^{-3})	σ_{GV} (mN·m^{-1})
1050	634.9	2.396	330.98
1100	300.6	2.387	328.98
1150	155.1	2.377	326.98

Four substrate materials were used: Glassy carbon, aluminum oxide (Al_2O_3), a platinum–rhodium alloy (PtRh) and a platinum–gold alloy (PtAu). Al_2O_3, PtRh and PtAu can withstand high temperatures without protective measures. Glassy carbon, however, reacts above 600 °C to form CO_2 when exposed to atmospheric oxygen. Since the

furnace used for our experiments (Thermo-Optical Measuring Instrument 1750/50, Fraunhofer Institute for Silicate Research) does not have an inert gas system, an improvised setup (see Figure 3) was constructed. A quartz glass beaker closed with a quartz glass lid was used as a sealed chamber. Two openings were provided in the lid—one for the outlet of the crucible and one for flushing the beaker with Argon (see Figure 3, right). Prior to the first measurements under Argon atmosphere (Argon of 99.998% purity and 20 ppm of other contaminant), the whole setup was tested with respect to the amount of residual oxygen. To this end, an oxygen measurement device (SGM5T, Zirox Sensoren und Elektronik GmbH, Germany) was used to measure the residual oxygen content inside the beaker. Beginning from 2.06×10^5 ppm at a time of t = 0 min, the oxygen content was slowly reduced to approx. 900 ppm within 6 minutes by flushing the beaker. To ensure the lower oxygen content during the experiment, a steady flow of Argon was applied. Residual oxygen contents lower than 900 ppm could not be reached even after flushing the beaker for more than an hour. Nevertheless, this concentration is sufficiently low to mostly avoid major oxidation of the glassy carbon during the experiments.

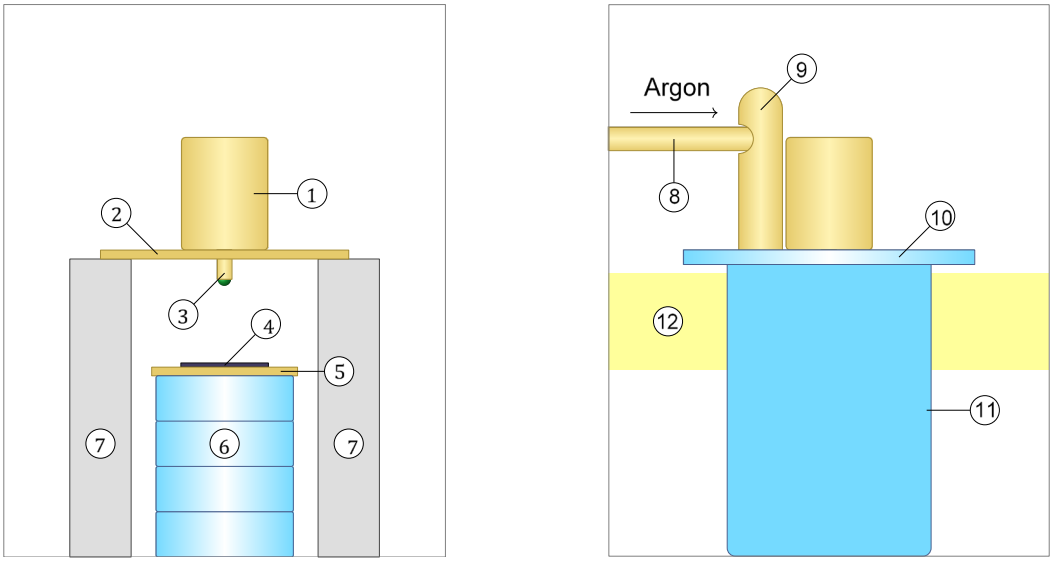

***Figure 3**. The system sketched above is placed inside an electrically heated furnace. Crucible (1) with outlet (3) is held by a perforated support (2) which rests on two refractory bricks (7). The outlet (3) has an inner diameter of approx. 5 mm. The sample (4) is placed on a stack of quartz glass cylinders (6) and an Al_2O_3 plate (5) which can also be positioned in a way to reach into the field of view of the camera (12). For experiments under argon a gas inlet is supplied via a tube (8) which is firmly connected to the furnace wall. The inert gas passes through a deflector (9) into a quartz glass beaker (11) containing the sample. The sample chamber is closed with a perforated quartz glass disk (10), which also serves as a crucible suspension.*

The general setup within in the furnace chamber comprises a funnel-like crucible that is suspended over a platelet-shaped specimen. The vertical distance between the crucible's outlet and the specimen is chosen so that both are in the camera's (Marlin F131B, Allied Vision Technologies GmbH with lens: Correctal® T/0.19, Sill Optics GmbH) field of view, which measures 44 mm by 33 mm.

Each experiment began by filling the crucible with approximately 0.35 g of cullet of the SLS glass. The exact amount of glass was determined in preliminary tests and ensures that a) exactly one droplet is formed and b) this droplet falls during the isothermal phase, i.e. at a constant temperature of either 1050 °C, 1100 °C or 1150 °C. The isothermal phase lasted for 180 minutes; heating and cooling took place at a rate of ±10 $K\cdot min^{-1}$ to avoid thermal shocks. Temperature was set via the furnace control panel and was verified with an external thermocouple (Type K). A droplet was formed purely by hydrostatic and gravitational forces. The camera recorded this process with a variable frame rate that adapts to the velocity of the molten glass. For example, the fall of the droplet (see Figure 4) was captured at 20 frames per second

(the camera's maximum frame rate), while a significantly lower temporal resolution was sufficient for the last hour of an experiment.

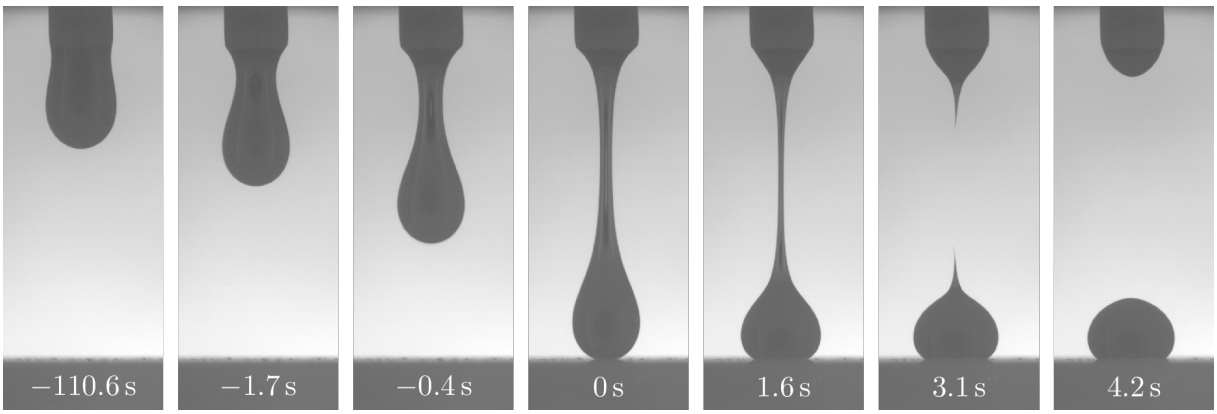

***Figure 4**. Formation and fall of a glass droplet. The time t = 0 s corresponds to the first contact of the glass with the material specimen. Due to spatial constraints, the drop–specimen contact happens before pinch-off (t = 3.1 s).*

A single experiment yielded around 400 grayscale images, which were then processed to optically determine the contact angle θ and spreading velocity *v*: First, the pixel contour of the specimen's surface was extracted through binarization and edge detection. The same image processing techniques also allowed the surface of the droplet to be identified. Next, the surface contours of the specimen and droplet were approximated by a line (with slope *m* and *y*-intercept *b*) and an ellipse (see Figure 3) [25], respectively. Once the parameters of both functions were known, the contact radius *r* and angle θ—where the mean value of θ was calculated from the left and right contact angles—could be calculated analytically [26]. As each image has a specific time stamp, the spreading velocity *v* was also readily available.

The acquisition and analysis of the images was automated using custom Python software. It relies on third-party libraries, most notably ls-ellipse, numpy, opencv-python, pymba and scipy and is available under the MIT license [27].

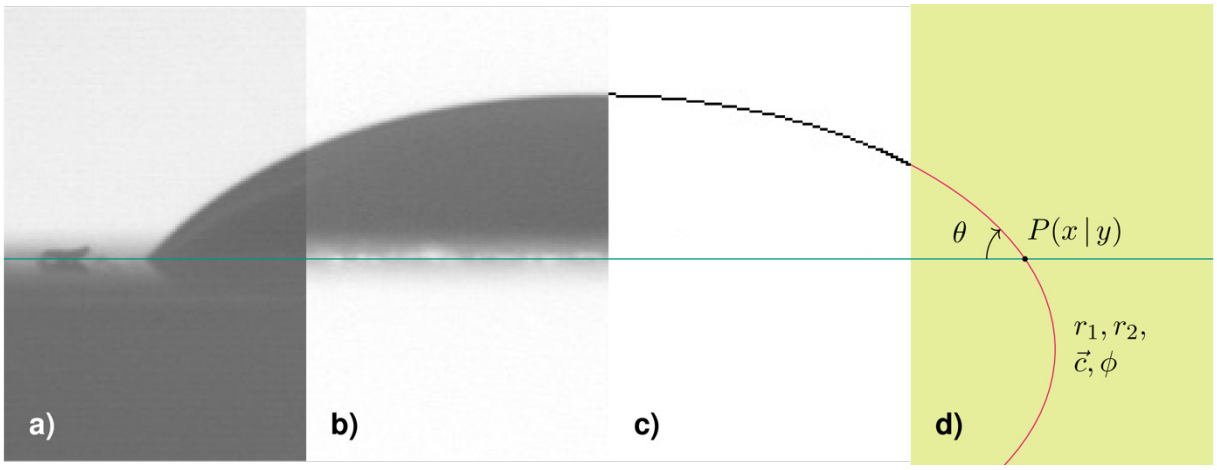

***Figure 5**. The same picture of a droplet at different stages of image processing. (a) The original grayscale image. The green line is an approximation of the specimen's surface and stems from an "empty" image that was taken before the droplet fell. (b) The droplet without the substrate. (c) The pixel contour of the droplet's surface, (d) which is approximated by a (rotated) ellipse with the radii r_1 and r_2, center $\vec{c}$ and angle Φ.*

3. Results

In the following, the spreading behavior (changing of contact angle) of the glass in contact to Al_2O_3, glassy carbon, PtAu and PtRh as a function of time and as a function of the capillary number is presented.

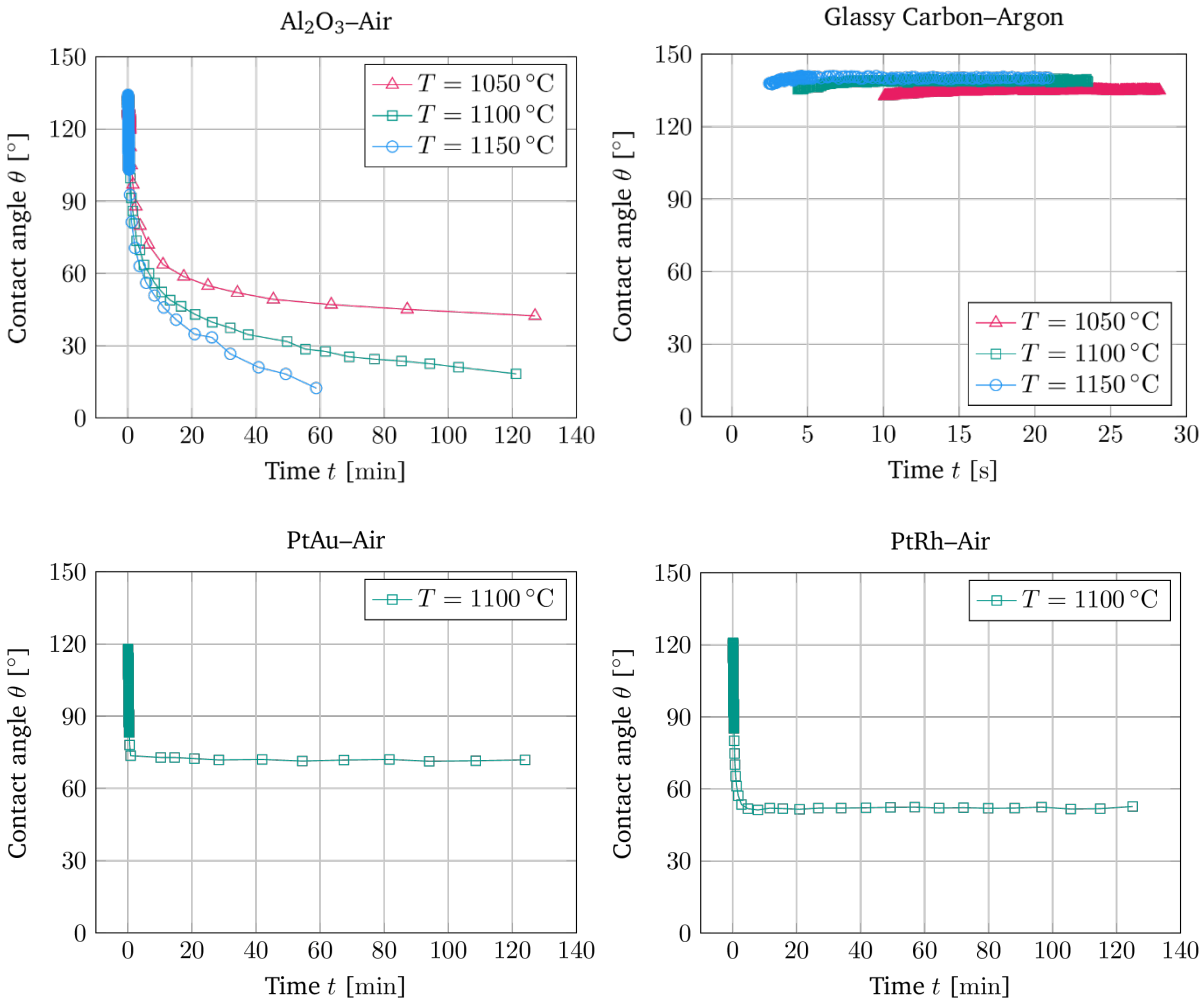

***Figure 6**. Contact angle of the glass in contact to Al_2O_3, glassy carbon, PtAu and PtRh as a function of time.*

On Al_2O_3 the spreading of the glass is not completed even after more than two hours. A slow and continuous spreading of the droplet is typical for a complete wetting behavior as is typical for silicate glasses on oxide ceramics. Since the static contact angle used in the Young's equation (equation 2) cannot be derived in this case, it is assumed to be close to 0°. On glassy carbon, the contact angle of the droplet slightly increases from 135° to 140° immediately after its constriction and reaches a constant value after a few seconds. The low wettability of the glassy carbon by the glass leads to large contact angles of more than 135° and to a small, almost constant contact radius. Because the latter hardly increases, the flattening of the settling droplet causes an initially increasing contact angle, the value of which is anti-proportional to the radius of the contact area. Hence, the increasing contact angle at the beginning can be seen as an artifact. For the PtAu and PtRh alloy, the mean contact angle of the droplet decreases very rapidly at the beginning of the spreading before it changes sharply to a static contact angle after about 3 min.

With the dynamic and static contact angle, spreading velocity and the respective glass-properties at hand, all necessary data is available to correlate the experimental data to the

molecular kinetic spreading model. For that, equation 9 is fitted to the contact angle depending on the capillary number. From this fitting procedure, the parameters k_s and λ can be obtained. As there are many steps involved—beginning with the image processing and ending with the fitting of Ca-contact angle-values—there are a lot of influences on the accuracy of the overall procedure, which are impossible to distinguish. Especially in the fit of the PtRh-Air-1100°C data, it becomes obvious that the molecular kinetic model underestimates the capillary number at large contact angles. As this high contact angles (and thus also high Ca-values) are obtained immediately after dripping onto the sample surface, the fitting might be off here due to the impact of the drop on the surface as kinetic energies of the free-falling drop are not considered in the molecular kinetic model. Nevertheless, to interpret the following figures—relating the capillary number Ca to the contact angle—it is helpful to consider Ca as a (scaled) spreading velocity *v* and to read the diagrams from right to left, i.e. along the time course. As for glassy carbon basically no dynamic contact angle exists, it is left out in the upcoming considerations.

For Al_2O_3, exemplarily data showcasing the dependency between contact angle and capillary number at two distinct temperatures of 1050 and 1100°C is presented together with a fitting curve according to equation 9 (see Figure 7). Additionally, the respective data for RhAu and RhPt are shown for a temperature of 1100 °C (also depicted in Figure 7).

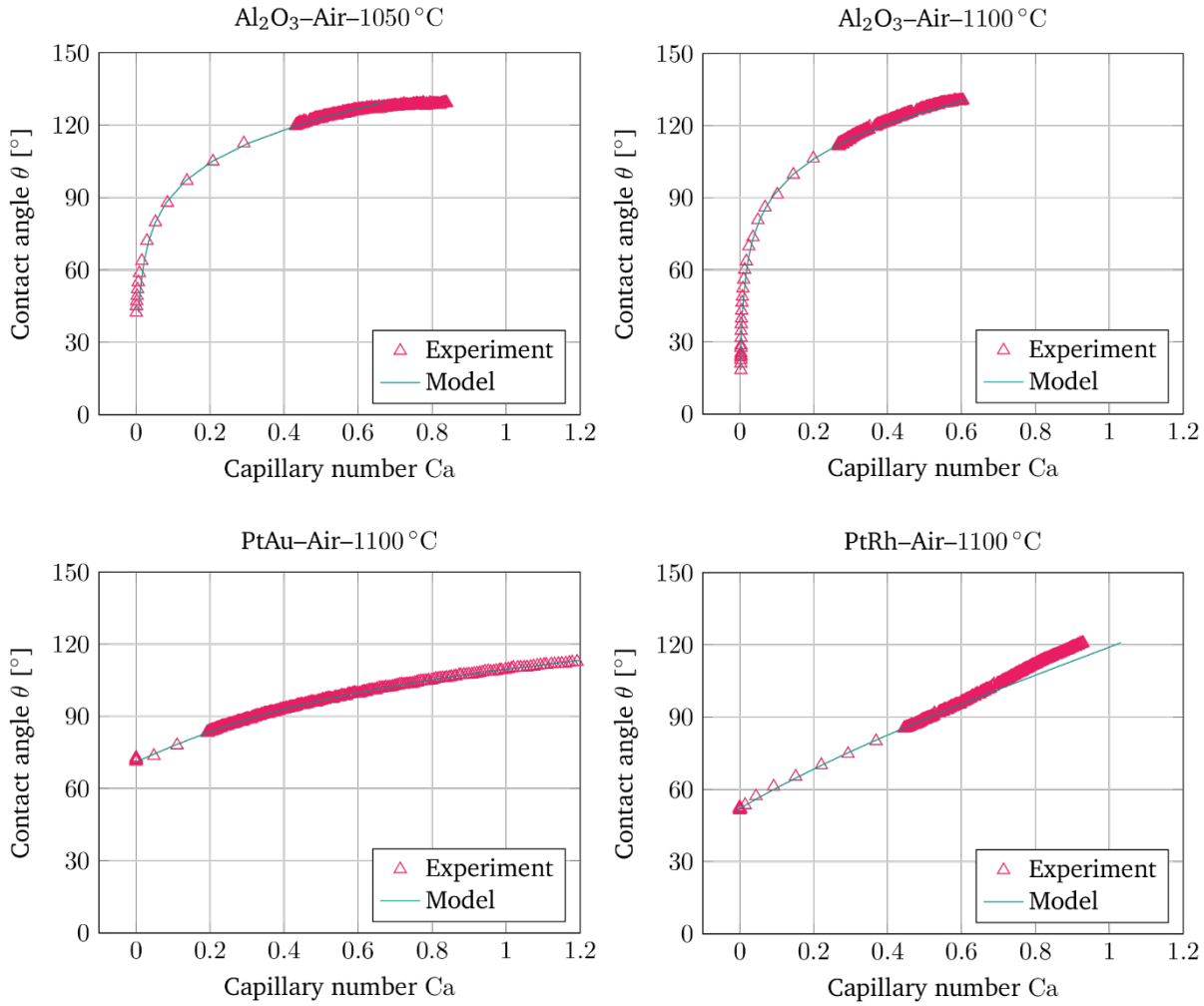

***Figure 7**. Contact angle θ of the glass in contact with aluminum oxide (Al_2O_3), glassy carbon, platinum-gold (PtAu) and platinum-rhodium (PtRh) as a function of the capillary number Ca together with the respective fitting curve according to equation 9.*

Rapid spreading is associated with an initially large contact angle which decreases over time, as does the spreading velocity or capillary number itself. Expressed the other way

around, the contact angle increases with capillary number, and on Al_2O_3 the increase is disproportionately large at small capillary numbers. The parameters k_s and λ as derived from the fit to the experimental data are summarized in Table 2:

Table 2. *Summary of the molecular kinetic parameters k_s and λ.*

Experimental conditions	**k_s [10^{11} Hz]**	**λ [Å]**
Al_2O_3 –Air–1050 °C	6.948	5.874
Al_2O_3–Air–1100 °C	7.547	5.865
Al_2O_3–Air–1150 °C	15.476	4.783
Al_2O_3–Argon–1050 °C	5.769	5.960
Al_2O_3–Argon–1100 °C	4.129	6.160
Al_2O_3–Argon–1150 °C	6.125	6.277
PtAu–Air–1100 °C	250.1	5.786
PtRh–Air–1100 °C	229.9	3.016

As can be seen in the plots in Figure 7, the molecular kinetic model shows a very good agreement with the measurement data. Although no corresponding literature data exist for the soda-lime glass used in in our experiments and for the other sample materials, Lopez-Esteban et al. [28] documented values for λ ranging from 1 to 4 Å for the spreading of a SiO_2-CaO-Al_2O_3 glass on pure molybdenum at 1200 °C. The jump distances λ ≅ 3–6 Å measured in this work are of the same order of magnitude and correspond approximately to the edge length of one to two SiO_4 tetrahedra. The hopping rate k_s is not separately in the publication by Lopez-Esteban et al. but instead values for the activation energy ΔG_0 of the molecular motions are given, which compared to the values in this work are lower by a factor of 2 to 3. This discrepancy can easily be attributed to the different temperatures used in the respective experiments. At the same time, the derived hopping rates of about 10^{12} Hz are in the range of molecular vibrational frequencies. Overall, the molecular kinetic model is in very good agreement with the measurement results and yields physically plausible values for the molecular jump rate k_s and jump distance λ.

The above presented results and theoretical considerations pave the way for rethinking the previously mentioned sticking hypothesis. The most decisive reasoning to refute this empirically derived adhesion theory of glass sticking at a given (fixed) viscosity mentioned at the beginning lies in the type of interaction between glass melt and contact material considered so far: It seems quite reasonable to conclude that in previous experiments it was not the actual metal surfaces that was examined as contact material, but rather the respective oxidized surfaces (also under inert gas, since oxide layers form very quickly, even if samples are only exposed to air for a short time). At first glance, this may not seem like a big difference. It is important to note here, however, that for a typical SLS-glass the oxygen-anion—due to their much larger diameter compared to cations—occupy most of the volume as can be seen in Table 3. Hence, they largely determine the interaction between the melt and contact material in the oxidized metal contact materials.

Table 3. *Volume fraction of the oxygen-ions and the metal-ions for the glass composition used in this work. Ionic radii after Pauling [29].*

	Mol % Elements	**Ionic radius [nm]**	**Ionic Volume [nm³]**	**Volume fraction [%]**
Si(IV+)	25.00	0.04	0.01	1.33
Ca(II+)	4.25	0.10	0.02	2.67
Na(+)	9.41	0.10	0.04	5.33
Al(III+)	0.83	0.05	negligible	negligible
Mg(II+)	1.32	0.07	negligible	negligible
O(II-)	59.19	0.14	0.68	90.67
	100.00		0.75	100.00

The same simple calculations can be done for the volume fraction of different metal cations in their respective oxides relative to the total ionic space in the structure. As a result, the metallic oxides also show the same ratios as calculated for the glass (see Table 3), given a certain oxidization state of the cation. For the above mentioned investigated Al_2O_3 the Al^{3+}-cations make up a volume fraction of approx. 8 vol% in the respective oxide. This once more validates the fact, that in the metal oxides the oxygen anions are by far taking most of the space of the structure as well and hence make up most of the surface in contact with the glass melt.

Due to the fact that many metal surfaces are easily oxidized, the interaction between glass-melt and metal surface is much more dominated by oxygen ions than by glass- or metal-cations. Consequently, as long as surface oxidization of the metal contact material is not largely prevented, as in the case of the Pt-alloys, the contact situation is nearly the same for all metals in contact with a glass melt: The oxygen anions of the glass interact with the oxygen anions of the oxidized metal, rendering the initial type of metal less significant. For example, by simply considering the ionic radii and ionic volume of the atomic components, a typical soda-lime-silica[1] glass yields a volume fraction of about 92% of Oxygen. The same calculations for the volume fraction of the different metal oxides, given a certain oxidization state of the metal-cation and depending on the structure of the respective metal, also show a similar relation as for the glass. For common metals used in glass forming, e.g. V, Cr, Ni, Cu, and Al all have volume fractions between 6 and 12 vol% in their respective oxides yielding a volume fraction of 88 to 94% of Oxygen. Zr for example being a bit of an exception with a volume fraction close to 20 vol%. This consideration shows in principle that also in the metal oxides, oxygen is often by far taking most of the space of the structure and hence most of the surface in contact to the glass melt.

4. Conclusion

As was shown, it is possible to determine glass-contact interaction at laboratory scale and correlate the results on a fundamental basis with a molecular kinetic model. Furthermore, the experiments showed that different contact materials indeed lead to different wetting, adhesion and sticking behavior *if* oxidization effects of the surface are taken into account. Generally speaking, one could sketch the glass and the metal oxide each as a condensed phase of oxygen ions with some metal ions in-between. For the glass the oxygen ions, or more precisely the electrons in the shells of the oxygen, therefore also strongly determine many properties based on e.g. the interaction with electromagnetic radiation such as optical properties. So, obviously, the oxygen is dominating both surfaces in the glass and in the substrate if the latter is oxidized.

[1] Calculated for a soda-lime-silica with main constituents of (in wt%) 70.6 SiO_2, 13.7 Na_2O, 11.2 CaO, 2.5 MgO and 2 Al_2O_3.

As a conclusion it is stated that there is no real independence of contact-material when it comes to glass-metal interaction such as sticking. Glass sticking rather is a question of surface-layer coverage by distinct elements. If present, anions are naturally dominating this interaction if e.g. oxidization is not suppressed by an inert atmosphere. As shown earlier, adhesion is mainly a question of Van-der Waals-interaction which can be related to contact angle dependencies. Hence, on a molecular level between glass and forming material, the true surface conditions and the Van-der-Waals interaction need to be considered. The polarizability and ionization potential seem to play an important role in sticking behavior and it can be assumed that a larger polarizability α means stronger interaction energy and stronger adhesion between the two contact partners according to the general equation for London-forces $\omega(r)_L$. As a result, this causes (more) sticking. This hypothesis will be the topic of a next publication.

In summary, the presented results show that the well-known hypothesis for sticking does not hold generally. Temperatures above the so-called sticking temperatures can be reached without the glass sticking to the contact-material. However, it has to be remarked that the interaction between metal substrates and hot glass under non-isothermal conditions is still not fully understood. The influence of temperature on sticking if metal oxides are present has to be investigated more closely and also the investigations need to be extended towards more glass contact partners to get a more complete picture. In the next stage, further contact materials will be investigated also avoiding oxidization of critical non-noble metals such as Fe, Ni and Cr. Also, non-isothermal control of the temperature of the substrate independent of the glass temperature will be considered in future experiments.

Author Contributions

Christian Roos: Conceptualization, Resources, Supervision, Writing – original draft;

Jan-Hendrik Veltmaat: Data curation, Formal analysis, Investigation, Software, Validation, Visualization, Writing – review & editing;

Philipp Jacobs: Conceptualization, Methodology, Project administration, Resources, Writing – original draft, Writing – review & editing.

Competing Interests

The authors declare that they have no competing interests.

Funding

No funds, grants or other support was received.

Acknowledgement

The author wishes to thank the laboratory staff of the Chair of Glass and Glass-Ceramics, RWTH Aachen University, for experimental support. The author wishes to thank Dr. Dominik Orzol for providing the pictures of Figure 1. This research did not receive any specific grant from funding agencies in the public, commercial, or not-for-profit sectors.

References

[1] U. Roger, “Untersuchung der Wechselwirkungen der bei der Glasformgebung eingesetzten Schmiermittel mit dem Formenmaterial und der Glasoberfläche sowie deren Einfluss auf den Wärmetransport”, Institut für Keramik, Glas und Baustofftechnik at TU Bergakademie Freiberg, 2008.

[2] H. J. Oel and A. Gottschalk, “Die Klebetemperatur zwischen Glas und Metallen”, Glastechnische Berichte, vol. 39, no. 7, pp. 319–323, 1966.

[3] M. P. Alekseenko, “Cohesion and adhesion of hot glass”, Mashinostroenie, 1969.

[4] B. G. Abramovich and G. E. Kalashnikov, “Sticking temperature of glass and molds”, Glass and Ceramics, vol. 38, no. 7, pp. 349–350, 1981. DOI: 10.1007/bf00710086.

[5] P. Manns, W. Döll, and G. Kleer, “Glass in contact with mould materials for container production”, Glass Science and Technology, vol. 68, no. 12, pp. 389–399, 1995.

[6] D. Rieser, P. Manns, G. Spieß, and G. Kleer, “Investigations on sticking temperature and wear of mold materials and coatings”, Advances in Fusion and Processing of Glass III, vol. 141, pp. 281–289, 2006. DOI: 10.1002/9781118405949.ch27.

[7] D. Rieser, G. Spieß, and P. Manns, “Investigations on glass-to-mold sticking in the hot forming process”, Journal of Non-Crystalline Solids, vol. 354, no. 12–13, pp. 1393–1397, 2008. DOI: 10.1016/j.jnoncrysol.2007.02.095.

[8] D. K. Orzol, C. Roos, and L. Wondraczek, “Tribological investigations of the glass-to-metal contact during glass forming at an industrial scale”, International Journal of Applied Glass Science, vol. 12, no. 3, pp. 381–390, 2021. DOI: 10.1111/ijag.15918.

[9] P. Heilmann and D. A. Rigney, “An energy-based model of friction and its application to coated systems”, Wear, vol. 72, no. 2, pp. 195–217, 1981. DOI: 10.1016/0043-1648(81)90367-7.

[10] P. Heilmann and D. A. Rigney, “Reply to comments on An Energy-Based Model of Friction and its Application to Coated Systems”, Wear, vol. 80, no. 3, pp. 385–386, 1982. DOI: 10.1016/0043-1648(82)90265-4.

[11] D. A. Rigney and P. Heilmann, “Reply to a comment on An Energy-Based Model of Friction and its Application to Coated Systems”, Wear, vol. 97, no. 3, pp. 306–309, 1984. DOI: 10.1016/0043-1648(84)90157-1.

[12] P. -G. de Gennes, F. Brochard-Wyart, and D. Quéré, “Capillarity and Wetting Phenomena”. Springer New York, 2004. DOI: 10.1007/978-0-387-21656-0.

[13] D. Bonn, J. Eggers, J. Indekeu, J. Meunier, and E. Rolley, “Wetting and spreading”, Reviews of Modern Physics, vol. 81, no. 2, pp. 739–805, 2009. DOI: 10.1103/revmodphys.81.739.

[14] D. E. Packham, “Theories of fundamental adhesion”, in Handbook of Adhesion Technology. Springer Berlin Heidelberg, 2011, pp. 9–38. DOI: 10.1007/978-3-642-01169-6_2.

[15] M. J. Davis and S. H. Davis, “Droplet spreading: Theory and experiments”, Comptes Rendus Physique, vol. 14, no. 7, pp. 629–635, 2013. DOI: 10.1016/j.crhy.2013.06.011.

[16] A. Marchand, J. H. Weijs, J. H. Snoeijer, and B. Andreotti, “Why is surface tension a force parallel to the interface?”, American Journal of Physics, vol. 79, no. 10, pp. 999–1008, 2011. DOI: 10.1119/1.3619866.

[17] C. E. Mortimer and U. Müller, Chemie, 9th ed. Stuttgart: Georg Thieme Verlag, 2008, ISBN: 978-3-13-484309-5.

[18] T. D. Blake and J. M. Haynes, “Kinetics of liquid/liquid displacement”, Journal of Colloid and Interface Science, vol. 30, no. 3, pp. 421–423, 1969. DOI: 10.1016/0021-9797(69)90411-1.

[19] R. Sedev, “The molecular-kinetic approach to wetting dynamics: Achievements and limitations,” Advances in Colloid and Interface Science, vol. 222, pp. 661–669, 2015. DOI: 10.1016/j.cis.2014.09.008.

[20] A. Fluegel, “Glass viscosity calculation based on a global statistical modelling approach”, Glass Technology: European Journal of Glass Science and Technology Part A, vol. 48, no. 1, pp. 13–30, 2007.

[21] A. Fluegel, “Global model for calculating room-temperature glass density from the composition”, Journal of the American Ceramic Society, vol. 90, no. 8, pp. 2622–2625, 2007. DOI: 10.1111/j.1551-2916.2007.01751.x.
[22] A. Fluegel, D. A. Earl, A. K. Varshneya, and T. P. Seward III, “Density and thermal expansion calculation of silicate glass melts from 1000 °C to 1400 °C”, Physics and Chemistry of Glasses: European Journal of Glass Science and Technology Part B, vol. 49, no. 5, pp. 245–257, 2008.
[23] A. Kucuk, A. G. Clare, and L. Jones, “An estimation of the surface tension for silicate glass melts at 1400 ◦C using statistical analysis”, Glass Technology, vol. 40, no. 5, pp. 149−153,1999.
[24] H. Salmang and H. Scholze, Keramik. Springer Berlin Heidelberg, 2007. DOI: 10.1007/978-3-540-49469-0.
[25] R. Halir and J. Flusser, “Numerically stable direct least squares fitting of ellipses”, in 6th International Conference in Central Europe on Computer Graphics and Visualization, World Society for Computer Graphics, 1998.
[26] M. C. Hendricks. “Rotated ellipses and their intersections with lines.” (2012), [Online]. Available: http://quickcalcbasic.com/ellipse%20line%20intersection.pdf (visited on 03/19/2024).
[27] J.- H. Veltmaat. “Software for the optical analysis of a glass droplet.” (2021), [Online]. Available: https://github.com/jhveltmaat/Drop-IT (visited on 03/18/2024).
[28] S. Lopez-Esteban, E. Saiz, J. S. Moya, and A. P. Tomsia, “Spreading of viscous liquids at high temperature: Silicate glasses on molybdenum”, Langmuir, vol. 21, no. 6, pp. 2438–2446, 2005. DOI: 10.1021/la0474621.
[29] U. Müller, Anorganische Strukturchemie (Studienbücher Chemie), 6th ed. Wiesbaden: Vieweg+Teubner, 2008. DOI: 10.1007/978-3-8348-9545-5.